Available online at www.sciencedirect.com
SCIENCE DIRECT®
ELSEVIER
Ultramicroscopy 94 (2003) 209–216
ultramicroscopy
www.elsevier.com/locate/ultramic

A novel STM-assisted microwave microscope with capacitance and loss imaging capability

Atif Imtiaz*, Steven M. Anlage

Center for Superconductivity Research, Department of Physics, University of Maryland, College Park, MD 20742-4111, USA

Received 20 March 2002; received in revised form 6 August 2002

Abstract

We report a new technique of scanning capacitance microscopy at microwave frequencies. A near field scanning microwave microscope probe is kept at a constant height of about 1 nm above the sample with the help of scanning tunneling microscope (STM) feedback. The microwaves are incident onto the sample through a coaxial resonator that is terminated at one end with a sharp tip (the same tip is used to conduct STM), and capacitively coupled to a feedback circuit and microwave source at the other end. The feedback circuit keeps the source locked onto the resonance frequency of the resonator and outputs the frequency shift and quality factor change due to property variations of the sample. The spatial resolution due to capacitance variations is $\cong 2.5$ nm. The microwave microscope is sensitive to sample sheet resistance, as demonstrated through measurements on a doped silicon sample. We develop a quantitative transmission line model treating the tip to sample interaction as a series combination of capacitance and sheet resistance in the sample.

PACS: +78.70.Gq; 84.37.+q; 07.79.C; 75.70.−i

Keywords: Scanning capacitance microscopy; Nanometer spatial resolution; Scanning tunneling microscopy (STM); Microwave microscopy; Near field

1. Introduction

Scanning capacitance microscopy can be used to map spatial variations of the topography of conducting materials, or the dielectric properites of thin films and bulk insulators [1–5]. In general, such microscopes detect a change in capacitance, δC, by means of a resonant circuit that includes the probe–sample capacitance. An early version of such a microscope employed a diamond stylus in contact with the sample. When the stylus was touching the sample, a probe electrode (attached to the stylus) was 20 nm above the sample. The electrode to sample capacitance was measured through the changing resonant frequency of an inductor/capacitor (LC) resonant circuit [1]. With this microscope, the lateral resolution claimed was 100 nm and vertical resolution of 0.3 nm. Other capacitance microscopes have been made by adding a similar resonant capacitance sensor to an atomic force microscope [2] and a scanning tunneling microscope [3] (STM). The lateral topographic resolutions reported were 75 and

*Corresponding author.
E-mail address: aimtiaz@squid.umd.edu (A. Imtiaz).

0304-3991/03/$ - see front matter
PII: S0304-3991(02)00291-7

25 nm, respectively. An interesting microwave frequency nonlinear capacitance microscope was integrated with STM to give spatial resolution of 5 nm [6]. These microscopes have been widely used for dopant profiling in semiconductors [6–9].

However, in many materials of interest, measurement of loss is crucial to extract the interesting physics. For example, certain colossal magnetoresistance (CMR) materials have "metallic" and "insulating" phases that coexist on very small (almost 1–2 nm) length scales [10]. In thin films of $Bi_2Sr_2CaCu_2O_{8+\delta}$, STM spectroscopic data show evidence for coexisting superconducting and semiconducting phases [11] on similar length scales. One way to distinguish between the two phases is to locally measure ohmic losses. Existing capacitance microscopes are not designed to image such quantities. A near-field microwave microscope would be the right tool, and can be utilized to quantitatively extract losses [12,13]. However, submicron spatial resolution is required to distinguish the finely intermixed phases.

The quantitative losses or sheet resistance (R_x) of a sample was extracted earlier [12] from the frequency shift and quality factor of the microscope resonator, with lateral resolution in the 10s to 100s of μm. We now want to improve the spatial resolution, while maintaining the sensitive loss imaging capability.

With a scanning microwave microscope, one can illuminate a controlled localized area of the sample with microwave fields and currents. In the past, some near-field microwave microscopes have utilized STM [14,15] or AFM tips [16–18] simply to concentrate RF electric field on a sample. The sharp end of the tip acts like a "lightening rod", enhancing the spatial resolution for microwave microscopy. In an earlier version of our microwave microscope, an STM tip was also used to focus electric fields on the surface [19]. Because the tip was in contact with the sample, with contact force of about 60 μN, the best spatial resolution achieved was $\simeq 1$ μm. The contact force flattened the imaging end of the tip, increasing the radius of curvature. One way to improve the spatial resolution of the microscope is to prevent the tip from touching the sample. To achieve this, the new version of the near-field microwave microscope (Fig. 1) has STM feedback integrated to maintain a roughly 1 nm constant height during scanning.

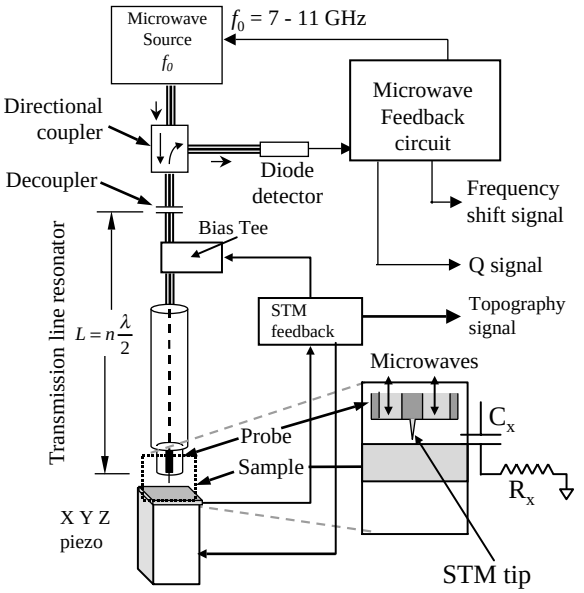

Fig. 1. Schematic diagram of the STM-assisted scanning near-field microwave microscope. A model of the probe–sample interaction is shown in the inset.

2. Experiment

The microscope, schematically presented in Fig. 1 is similar to the versions discussed at length in prior publications [19–23]. Changes made to our microscope include using a bias tee to make the DC connection to STM feedback while maintaining an AC coupling to the microwave source and feedback circuit. Also, the sample is now on an XYZ piezoelectric (piezo) translation stage, instead of an XY motor stage. At one end of the coaxial resonator is an open ended coaxial probe with a sharp STM tip sticking out of its center conductor. As with our previous microscopes [19], the other end of the resonator is capacitively coupled to a microwave source and a feedback circuit via a directional coupler and a diode detector, as shown in Fig. 1. The feedback circuit keeps the source locked onto the resonance frequency f_0, of the resonator and it gives the frequency shift (Δf) and quality factor (Q) as

output signals. However, the probe–sample separation is maintained by a constant current STM feedback loop during scanning.

Many interesting materials have transition temperatures well below room temperature, requiring a cryogenic microscope. We use a commercially available Oxford Cryostat to cool the sample and part of the microscope. The sample can be cooled to any temperature between 4.2 K and room temperature. The quality factor of the microscope is enhanced at low temperatures due to the decrease of microwave losses in the resonator.

3. Model

The inset of Fig. 1 shows a closer look at the tip to sample interaction. This interaction is modeled as an effective capacitance C_x in series with the losses in the conducting sample due to ohmic dissipation, R_x. The complex load impedance presented to the microscope is $Z_x = R_x + (1/i\omega C_x)$.

Our quantitative understanding of the microscope is based on a transmission line model developed earlier [20,21]. In this model, the frequency shift and Q of the microscope depend both on C_x and R_x. In the region of interest, an estimate (discussed below) for the capacitance at a height of 1 nm is $C_x \simeq 10$ fF, giving a capacitive reactance ($Im[Z_x]$) on the order of 2 kΩ at 7.5 GHz. For situations where C_x is not too large (roughly C_x values $\leqslant 10$ fF), we can approximate the model frequency shift as $\Delta f = -bC_x$, independent of R_x, where b depends on microscope geometry. The model Q depends on C_x^2 as $Q = Q_{\max} - d(R_x)C_x^2$, where $Q_{\max}$ is the microscope Q with no sample present. For increasing R_x this slope increases in magnitude, roughly as $d(R_x) \sim R_x$. To summarize, in this small capacitance limit, the frequency shift image can be regarded as a capacitance image, and the Q image will contain contributions from both capacitance C_x and losses R_x. Similar results are obtained from a lumped element model in which the resonator is treated as a parallel RLC circuit.

In both models of the microscope we find, in general, that the minimum in Q versus R_x [12,21] is always at the point where $\omega C_x R_x = 1$. Hence the sensitivity of our microscope to sample losses is determined in part by the value of the probe–sample capacitance. Other observations about the qualitative behavior of Δf and Q with sample properties have been discussed at length in prior work [12,20].

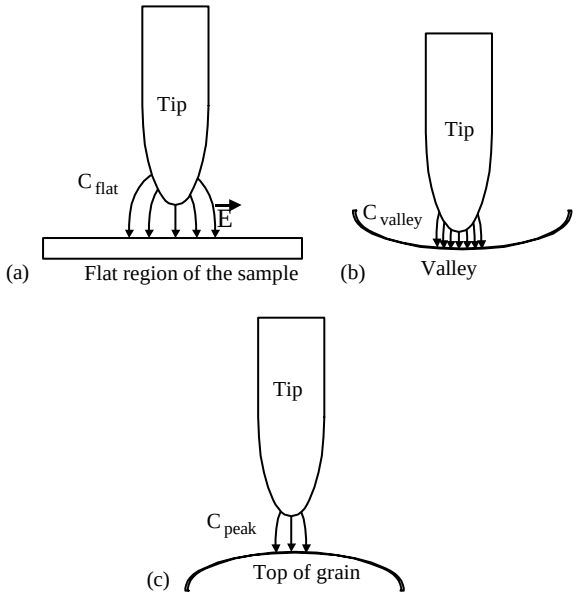

Fig. 2. Schematic of (a) Tip above flat region of the sample; (b) Tip in a valley; and (c) Tip above a grain. The relative capacitance values between the tip and the sample are $C_{\text{peak}} < C_{\text{flat}} < C_{\text{valley}}$.

Qualitatively, we expect C_x, to be large in a valley and small near a peak on the sample surface, as shown in Fig. 2. The capacitance between tip and sample can be calculated by assuming that the tip acts like a metallic sphere above a metallic infinite plane [24]. Naively, we expect the spatial resolution for capacitance variations to be on the order of the radius of the sphere.

4. Results

We find that the value of capacitance between tip and sample strongly depends on the geometry of the tip. We have used Pt–Ir alloy cut tips, as well as Pt–Ir alloy etched tips and W etched tips. All three tips have significantly different

geometries. The W tip shows the largest Δf contrast as a function of height between tunneling and 2000 nm from the surface (Fig. 3). For this tip we have seen a frequency shift slope $d(\Delta f)/dz|_{z\to 0}$ contrast of roughly 0.3 kHz/nm over a thin gold film deposited on a mica substrate. The etched Pt–Ir tip has a smaller contrast of 0.075 kHz/nm, but still larger than a cut Pt–Ir tip, which has a contrast of 0.025 kHz/nm, all on the gold on mica thin film (all three tips are compared in inset of Fig. 3). The largest frequency shift that we have seen is 800 kHz between tunneling height and 500 nm, over an oxidized titanium thin film sample with an etched W tip. The experiments were carried out around 7.5 GHz with a resonator of length 1.06 m.

To quantitatively understand the frequency shift versus height data, we calculate capacitance for a given sphere radius and height above the sample starting from a typical tunneling height of 1 nm and extending to 2000 nm. The values are fed into the transmission line model [20,21], which calculates the frequency shift. The inset of Fig. 3 shows the fit based on this model to the frequency shift versus height data for etched W and Pt tips over the gold/mica sample. The sphere radius was used as the fitting parameter, and Fig. 3 shows that the W tip data fits well for a sphere of radius 27 μm, while the etched Pt tip fits with a sphere of 10 μm. These values for tip radius fits are comparable to those seen by other researchers [18,24] and give probe–sample capacitance on the order of 1–10 fF at tunneling heights. We find, however, that the Pt–Ir cut tip is irregular and does not fit the sphere above the plane model.

Fig. 4 shows simultaneously acquired images of STM topography and microwave properties on a $La_{0.67}Ca_{0.33}MnO_3$ CMR thin film. The STM topography clearly shows the granular structure of the film. The total height variation is about 175 Å, and the smallest grain is about 285 Å on each side. The simultaneously acquired frequency shift data shows all the same granular features, with similar spatial resolution. Note that the frequency shift is more negative for the region between the grains, and less negative for regions near the top of the grains, as expected from Fig. 2.

Surprisingly, the Δf and Q image spatial resolution is just as good as STM topography. The contrast in Δf and Q come largely from the

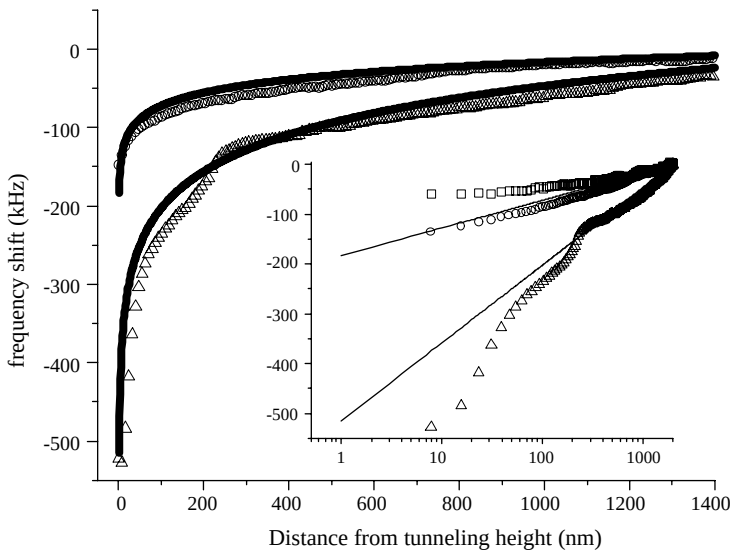

Fig. 3. Comparison of frequency shift vs. distance from tunneling height data for Pt–Ir etched (open circles) and W etched tips (open triangles) to the sphere above the plane model (solid lines). Experiments were performed at 7.37 GHz. Inset plots the frequency shift versus log z to show the logarithmic distance scaling from the sphere above the plane capacitance model. The data are normalized to Δf (2000 nm) = 0 kHz. The inset also shows data for Pt–Ir cut tip (hollow squares), performed at 7.25 GHz. The sample is a thin gold film on mica substrate.

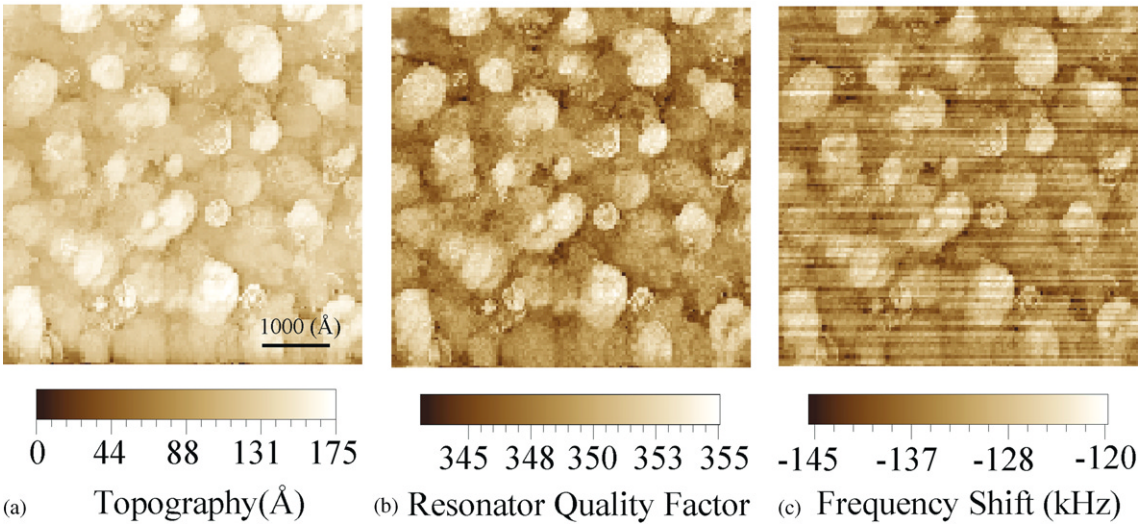

Fig. 4. Simultaneously acquired (a) topography; (b) quality factor; and (c) frequency shift image of $La_{0.67}Ca_{0.33}MnO_3$, thin film which is 1000 Å thick on $LaAlO_3$ substrate. The images are 6000 Å on each side. Data is taken at 272 K with a Pt–Ir etch tip at 7.67 GHz. Sample bias was 1 V and tunnel current set point was 1 nA. Streakiness in the frequency shift image is due to drift in the microwave source frequency.

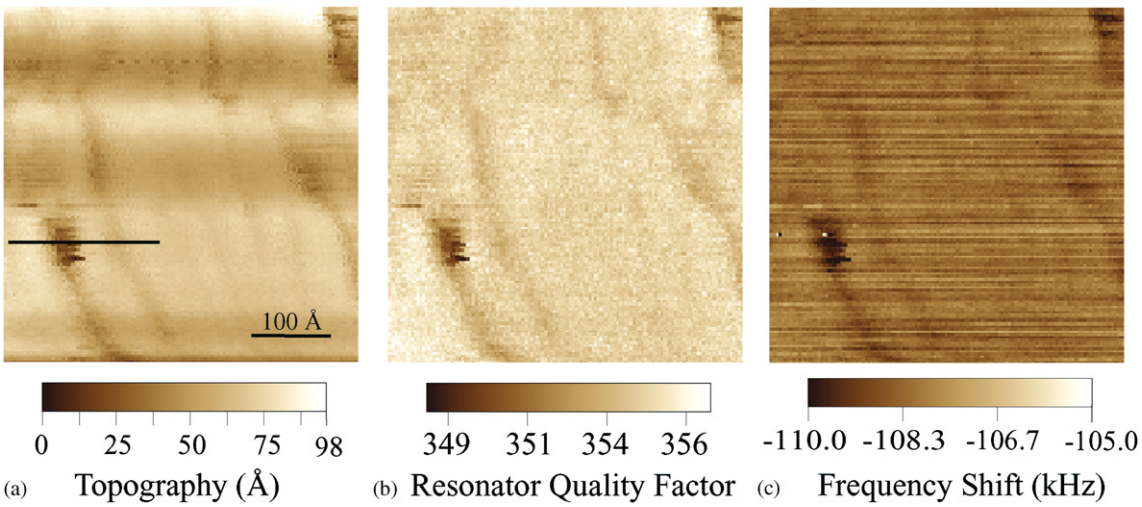

Fig. 5. Images of the top of one grain of a $La_{0.67}Ca_{0.33}MnO_3$ (a) STM topography; (b) quality factor; and (c) frequency shift images. Image size is 492 Å on each side. The horizontal light and dark wide bands on the STM topography image are due to temperature drift of the apparatus. The microwave data is not sensitive to this drift because the capacitance is only sensitive to tip–sample separation. Data is taken at 240 K with a Pt–Ir etch tip at 7.67 GHz. The horizontal line cut in (a) is shown in Fig. 6. The sample bias was 1 V and tunnel current set point was 1 nA. Streakiness in the frequency shift image is due to drift in the microwave source frequency.

topography-following mode, where STM feedback is maintaining a constant tunnel current. As the tip goes into a valley on the surface, the microwave microscope will see an increase in capacitance between the tip and sample (Fig. 2) which will produce a more negative frequency shift. A drop in

Q is also seen due to the increase in C_x and possibly also due to a change in R_x, as proposed [25] for CMR thin films.

Fig. 5 shows the data on the top of one grain of the $La_{0.67}Ca_{0.33}MnO_3$ film, shown in Fig. 4. This image is 492 Å on each side and the overall STM topography is 96 Å. The simultaneously acquired frequency shift image ranges from -105 to -110 kHz and the Q image ranges from 348 to 357. The dark lines in the topography image are narrow dips about 8–10 $La_{0.67}Ca_{0.33}MnO_3$ crystallographic unit cells deep (unit cell size is 3.86 Å). The Q and frequency shift images clearly show these dips as well. Fig. 6 shows the line cut through the largest dip in Fig. 5, where the topography shows that this feature is 55 Å deep, from the top of the grain. The frequency shift change is about 2 kHz and Q drops from 356.5 to 348.5 over this feature. One can regard Fig. 5 as a relatively flat region of the sample where the microscope shows a baseline frequency shift, $\Delta f \sim -105$ kHz. When the tip moves into the 5.5 nm deep valley (Fig. 6), under STM constant-current mode, the microwave microscope shows an additional drop of ~ 2 kHz in frequency shift, giving a slope, $d(\Delta f)/dz \sim 0.3$ kHz/nm, consistent with the results shown in

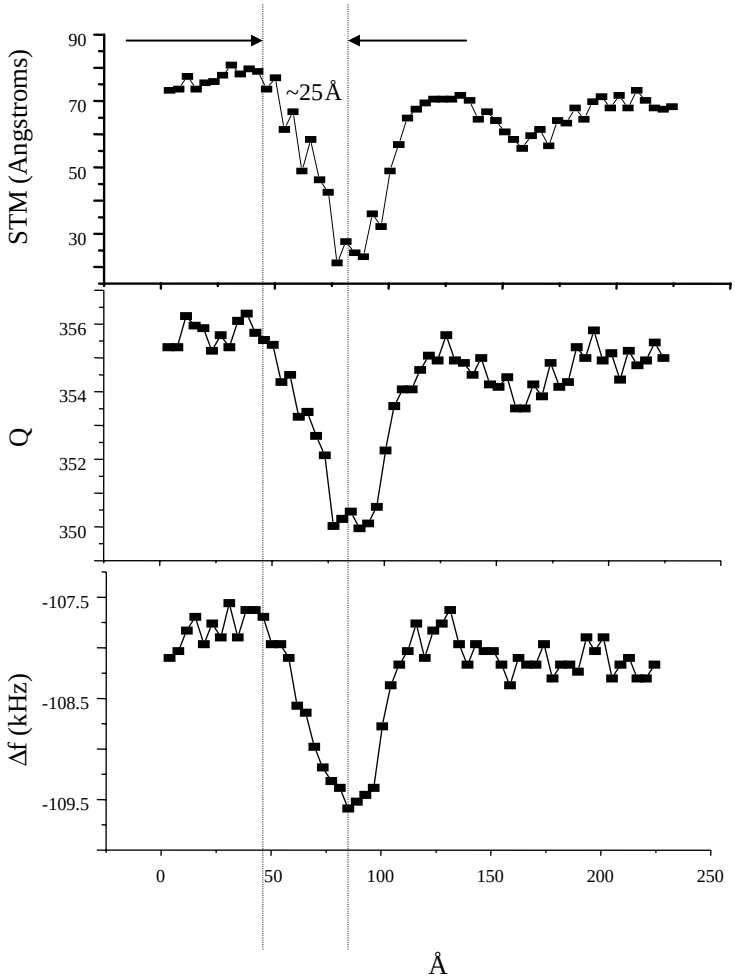

Fig. 6. Line cut of the data shown in Fig. 5. It demonstrates a 25 Å lateral spatial resolution for capacitance variations in the microwave response of the sample.

Fig. 3 for the frequency shift contrast near the surface.

This analysis suggests that the lateral spatial resolution is not limited by the radius of the sphere used to estimate the probe–sample capacitance [24]. Instead, the spatial resolution is dictated by the capacitance variations imposed through STM constant-current mode. Comparing the three line cuts through the feature in Fig. 6, we clearly see that the spatial resolution for capacitance variations of the microwave microscope is comparable to STM, and is no worse than 25 Å. This is consistent with estimates of ultimate sharp-tip spatial resolution in the literature [5].

However, the microwave microscope is also sensitive to physical properties, such as losses, of the sample. This is best illustrated in an experiment performed over a boron-doped silicon sample, where 2 μm wide doped regions are separated by stripes of undoped silicon of varying widths. The doped regions of the sample have a concentration of 1×10^{19} atoms/cm^3 with 100 nm thickness. The doped regions have a sheet resistance of about $R_x = 2$ kΩ [26]. We see from Fig. 7, that frequency shift is more negative over the doped region and the Q is lower, which is consistent with our expectation [21], since the doped region is close to the limit of $\omega C_x R_x = 1$ and the undoped region has $\omega C_x R_x \gg 1$. The images in Fig. 7 clearly demonstrate that the frequency shift and Q differentiate between the doped and undoped regions, while STM topography (at high sample bias) does not distinguish the two regions. The STM topography is mainly due to tilt and damage on the surface of the sample. Hence, the microwave microscope can make topography-free maps of physical properties.

Noise ultimately limits our sensitivity to capacitance variations. There is noise in both the STM positioning system and the microwave microscope. At room temperature, the estimated position noise of the z piezo is 0.35 Å and the position noise in the x and y directions is 1.2 Å. This translates to 0.0026 kHz of noise in Δf and 0.0083 in Q for a typical Pt-etch tip, so we conclude that the contribution to noise from the positioning system is negligible. We find that for the microwave microscope, sitting far away from the sample, the jitter seen in the frequency shift signal is about 0.5 kHz, and the variation in Q is about 0.1 out of 383. The lock-in time constant was 1 ms for these experiments.

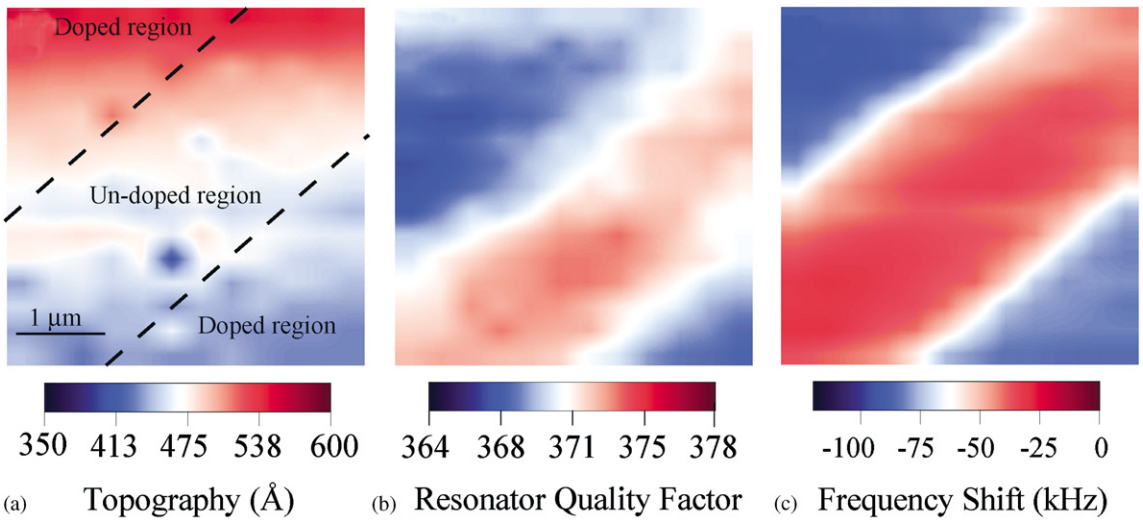

Fig. 7. Images of a boron doped silicon sample (a) STM topography; (b) Quality factor; and (c) frequency shift images. The dashed lines and labels on the STM image show where the doped and undoped regions are located on the sample. The quality factor and frequency shift images show the three regions clearly, while the STM topography is mainly due to tilt and the damaged surface. Sample bias was 3.8 V and tunnel current set point was 0.5 nA.

5. Conclusions

We have demonstrated a novel microwave frequency scanning capacitance microscope with spatial resolution of no worse than 25 Å. The microwave contrast depends strongly on the tip–sample capacitance. This capacitance depends strongly on the geometry of the tip. This scanning capacitance microwave microscope can serve as a high-resolution platform for doing other kinds of measurements, such as local loss and local nonlinear properties of semiconductors [6] and superconductors [27,28].

Acknowledgements

This work has been supported by an NSF SBIR-II subcontract from Neocera, Inc. under NSF DMI-0078486, an NSF Instrumentation for Materials Research Grant DMR-9802756, the University of Maryland/Rutgers NSF-MRSEC shared experimental facility under Grant number DMR-00-80008, the Maryland Industrial Partnerships Program 990517-7709, and by the Maryland Center for Superconductivity Research. We acknowledge Amlan Biswas for providing us with the $La_{0.67}Ca_{0.33}MnO_3$ film and Ellen Williams for providing the doped silicon sample.

References

[1] J.R. Matey, J. Blanc, J. Appl. Phys. 57 (1985) 1437.
[2] R.C. Barrett, C.F. Quate, J. Appl. Phys. 70 (1991) 2725.
[3] C.C. Williams, W.P. Hough, S.A. Rishton, Appl. Phys. Lett. 55 (1989) 203.
[4] S. Lanyi, J. Torok, P. Rehurek, Rev. Sci. Instrum. 65 (1994) 2258.
[5] S. Lanyi, J. Torok, P. Rehurek, J. Vac. Sci. Technol. B 14 (1996) 892 and references therein.
[6] J.-P. Bourgoin, M.B. Johnson, B. Michel, Appl. Phys. Lett. 65 (1994) 2045.
[7] W. Seifert, E. Gerner, M. Stachel, K. Dransfeld, Ultramicroscopy 42–44 (1991) 379.
[8] J.S. McMurray, J. Kim, C.C. Williams, J. Vac. Sci. Technol. B 16 (1998) 344.
[9] J.J. Kopanski, J.F. Marchiando, J.R. Lowney, Mater. Sci. Eng. B 44 (1997) 46.
[10] A. Moreo, S. Yunoki, E. Dagotto, Science 283 (1999) 2034.
[11] T. Cren, D. Roditchev, W. Sacks, J. Klein, J.-B. Moussey, C. Deville-Cavellin, M. Lagues, Phys. Rev. Lett. 84 (2000) 147.
[12] D.E. Steinhauer, C.P. Vlahacos, S.K. Dutta, F.C. Wellstood, S.M. Anlage, Appl. Phys. Lett. 72 (1998) 861.
[13] F. Duewer, C. Gao, I. Takeuchi, X.-D. Xiang, Appl. Phys. Lett. 74 (1999) 2696.
[14] S.J. Stranick, P.S. Weiss, Rev. Sci. Instrum. 65 (1994) 918.
[15] B. Knoll, F. Keilmann, A. Kramer, R. Guckenberger, Appl. Phys. Lett. 70 (1997) 2667.
[16] D.W. van der Weide, Appl. Phys. Lett. 70 (1997) 677.
[17] Y. Cho, S. Kazuta, K. Matsuura, Appl. Phys. Lett. 75 (1999) 2833.
[18] H. Odagawa, Y. Cho, H. Funakubo, K. Nagashima, Jpn. J. Appl. Phys. 39 (2000) 3810.
[19] D.E. Steinhauer, C.P. Vlahacos, F.C. Wellstood, S.M. Anlage, C. Canedy, R. Ramesh, A. Stanishevsky, J. Melngailis, Appl. Phys. Lett. 75 (1999) 3180.
[20] C.P. Vlahacos, R.C. Black, S.M. Anlage, A. Amar, F.C. Wellstood, Appl. Phys. Lett. 69 (1996) 3272.
[21] D.E. Steinhauer, Quantitative imaging of sheet resistance, permittivity, and ferroelectric critical phenomena with a near field scanning microwave microscope, Ph.D Thesis, University of Maryland, 2000 (Chapter 3).
[22] D.E. Steinhauer, C.P. Vlahacos, F.C. Wellstood, S.M. Anlage, C. Canedy, R. Ramesh, A. Stanishevsky, J. Melngailis, Appl. Phys. Lett. 71 (2000) 2751.
[23] D.E. Steinhauer, S.M. Anlage, J. Appl. Phys. 89 (2001) 2314.
[24] C. Gao, F. Duewer, X.-D. Xiang, Appl. Phys. Lett. 75 (1999) 3005 and references therein.
[25] A. Biswas, M. Rajeswari, R.C. Srivastava, Y.H. Li, T. Venkatesan, R.L. Greene, Phys. Rev. B. 61 (2000) 9665.
[26] S.M. Sze, Physics of Semiconductor Devices, Wiley, New York 1969, p. 43.
[27] Sheng-Chiang Lee, S.M. Anlage, Study of local nonlinear properties using a near-field microwave microscope, IEEE Trans. Appl. Supercond., 2003.
[28] Sheng-Chiang Lee, S.M. Anlage, Spatially resolved nonlinearity measurements of $YBa_2Cu_3O_{7-\delta}$ Bi-crystal grain boundaries, Appl. Phys. Lett., 2002, submitted.